Analysis of an Actively Twisted Rotor by Multi-Body Global Modelling

Gian Luca Ghiringhelli, Pierangelo Masarati[1] and Paolo Mantegazza

Politecnico di Milano,
Dipartimento di Ingegneria Aerospaziale,
via La Masa 34, 20158, Milano, ITALY
Tel.: ++39(02)2399-8393
Fax: ++39(02)2399-8334

Abstract.

The paper presents a procedure and the integrated tools for the aeroelastic analysis of an Active Twist helicopter Rotor (ATR). The active twisting of rotor blades is carried out by induced-strain actuators distributed into the structure of the blade. Active fibre composites (AFC), made of piezoelectric fibres actuated by interdigitated electrodes (IDE), are used to obtain anisotropic induced-strain actuation capable of twisting the blade. The elastic, inertial and piezoelectric properties of the blade section are determined by a dedicated semianalytical formulation that accounts for the non-homogeneity and the anisotropy of the elastic and piezoelectric materials. A three-dimensional FEM analysis of the piezoelectric fibre with IDE is used to estimate the equivalent material properties required for the blade section characterisation. A four-blade, articulated rotor is analysed in hover and forward flight conditions. The system is modelled by an original multi-body formulation, implemented in a code named MBDyn (Multi-Body Dynamics). The equilibrium equations and the definitions of the momenta are written for each body, together with the constraint equations, in the spirit of a Redundant Coordinate Set formulation. The blades are modelled as beam elements, by an original finite volume formulation for the analysis of nonlinear, initially curved and twisted beams subject to large displacements and rotations. The formulation is extended to include the effects of embedded piezoelectric devices as actuators. Electric and control-related degrees of freedom and elements have been added to MBDyn. Preliminary results related to the actuation authority of the active blade are presented

Keywords: Active Fiber Composites, Active Twist Rotor, Beam Analysis, Multi-Body Dynamics, Rotorcraft Analysis

Introduction

The work is articulated in the following phases: (a) recognition of the need for induced twist in beam-like structures, and identification of the means to obtain it, (b) determination of the piezoelectric properties of an elementary cell, made of a portion of a single piezoelectric fibre between two adjacent electrodes, embedded in an epoxy matrix with reinforcing fiberglass, (c) determination of the properties of an equivalent piezoelectric material, (d) characterisation of the section of a blade with embedded AFC actuators, and (e) dynamic analysis of the active blade in a typical active twist rotor blade application.

Active Twist Control

The strain-induced twisting of a slender body, like a rotor blade, requires the ability to induce shear strains in the beam section, that result in a global twist of the structure. A very promising material for distributed and embedded induced strain actuation has been found in the piezoelectrics. The piezoelectric effect is represented by the capability of a material to produce an electric field when loaded, and, on the contrary, to deform when subject to an electric field. In usual notation [17],

[1]Author for correspondence, E-mail: *masarati@aero.polimi.it*

the linearised piezoelectric constitutive law is:

$$\left\{ \begin{array}{c} S \\ D \end{array} \right\} = \left[\begin{array}{cc} s^{(E)} & d^T \\ d & \epsilon^{(T)} \end{array} \right] \left\{ \begin{array}{c} T \\ E \end{array} \right\} \tag{1}$$

where $S_{6\times1}$ and $T_{6\times1}$ are the strain and stress arrays, and $E_{3\times1}$ and $D_{3\times1}$ are the electric field and the electric displacement arrays. Piezoeletric devices for distributed induced strain applications are manufactured in two-dimensional laminæ, to be applied on, or embedded into, the passive, or host, structure. The usual implementation consists in thin, thickness-wise (direction 3) polarised laminæ, that show an isotropic behaviour in their plane, thus being unable to induce the desired twisting. In fact, the shear strain in the plane of the piezoelectric lamina is:

$$\gamma_{xy} = 2\cos(\alpha)\sin(\alpha)(S_1 - S_2) \tag{2}$$

where the y and z axes lie in the plane of the beam section and x is the axis of the beam, while S_1 and S_2 are the principal strains in the plane of the piezoelectric in the material frame and α is the relative angle between the material and the beam reference frames, resulting in no shear when the two induced strains, S_1 and S_2, are equal. An in-plane anisotropic piezoelectric material is required to obtain different electrically induced strains in directions 1 and 2. A material with such properties has been obtained by applying the fibre composite technology to the ceramic piezoelectric material, resulting in the Active Fibre Composites (AFC) [1]. Subsequent research led to the development of the Inter-Digitated Electrodes (IDE) principle [16] as a useful means to induce anisotropic in-plane actuation. The electrodes are aligned in pairs of conductive strips on both the upper and the lower surface of the piezoelectric. The pairs of strips are alternately charged planewise, so that an alternate, in-plane electric field normal to the strips is generated. The piezoeletric material is initially polarised by means of the strips themselves during the manufacturing process. The resulting device exploits the main piezoelectric coupling coefficient (d_{11}), which is usually larger than the secondary ones ($d_{12,13}$) and opposite in sign ($d_{12,13} = -kd_{11}$, with $k \simeq 0.2 \div 0.5$); both the fibres and the polarisation are in direction 1. When used in conjunction with AFC, the interdigitated electrodes can apply the control tension exactly in the direction of the fibre, thus completely decoupling the induced strain in the direction on the fibre from the strains in the other directions. The electrically induced strain is applied in the direction of the piezoelectric fibres only, resulting in a truly anisotropic actuation in the plane of the active ply. Equation 2 shows that when the fibres are oriented 45^o degrees apart from the beam axis, and the two normal strains differ, the maximal coupled axial-shear actuation of the ply is obtained; the axial actuation loads can be cancelled by stacking the active plies oriented 90^o apart from each other.

Material Characterisation

The characterisation of a composite material is a complex topic. Different techniques have been developed to predict the elastic properties of a fibrous composite material starting from the elastic properties of its components, namely the fibres and the matrix [4]. Extensions to the case of thermoelectroelastic materials have been proposed in the literature [5, 6]. Such analytical models rely on the symmetry and the simplicity of the analytical modelling of a single, indefinitely long fibrous inclusion. The case of the AFC with IDE is far more complicated due to the peculiar geometry of the electrodes, that add a higher degree of complexity to the behaviour of the material. A ply of AFC material is usually made of a single layer of piezoelectric fibres, bounded to two thin films that carry the electrode patterns. It represents a three-dimensional, discrete, repetitive structure both from the mechanical and the electric standpoint. As a consequence, the elastic and electric fields are fully three-dimensional and periodical, due to the repetitivity of the pattern of the fibres in direction 2 and of the electrodes in direction 1. The present technology allows the manufacturing of one-fibre thick plies of the order of 0.10 mm [1]. The granularity of the repetitive pattern is such that, from a macroscopic point of view, an equivalent, homogeneous orthotropic piezoelectric material is expected to exist, and to be able to capture the fundamental behaviour of the AFC material. Here an attempt is made to predict the properties of such corresponding

Table 1: *Equivalent material properties*

Property	Circular	Rectangular	
C_{11}	11.99e6	12.11e6	[psi]
C_{12}	0.98e6	2.14e6	[psi]
C_{13}	1.06e6	2.93e6	[psi]
C_{22}	3.57e6	6.15e6	[psi]
C_{23}	0.93e6	2.26e6	[psi]
C_{33}	3.91e6	8.14e6	[psi]
C_{44}	1.16e6	2.36e6	[psi]
C_{55}	2.45e6	0.78e6	[psi]
C_{66}	2.41e6	0.29e6	[psi]
e_{11}	8.02e-9	1.26e-6	[psi in/V]
e_{12}	-6.74e-10	-4.00e-8	[psi in/V]
e_{13}	-8.72e-10	-6.06e-8	[psi in/V]

continuum, by conventional electroelastic Finite Element Analysis (FEA). By exploiting the symmetry of the piezoelectric component, a finite portion of fibre, comprised between the centerlines of two rows of electrodes, is modelled by a commercial FEA code; the FE models are shown in Figure 1. The figure refers to the circular section fibre presently investigated at MIT [1] and to the

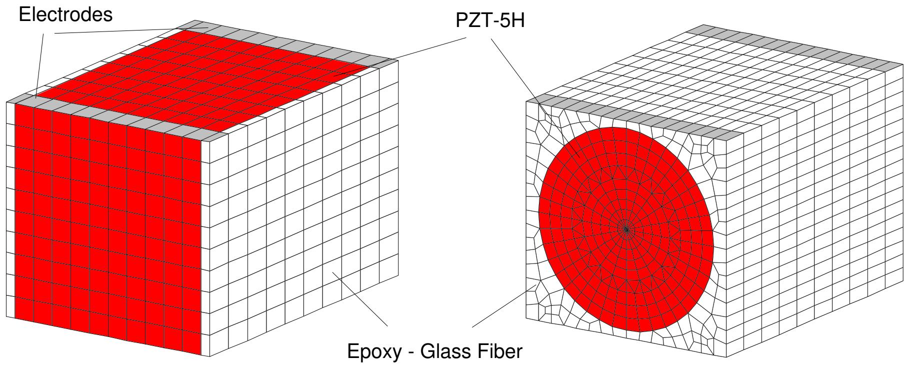

Figure 1: *FE models of the two specimen*

rectangular section fibre under investigation at NASA LaRC [22]. The latter geometry seems to be more promising in terms of ease of manufacturing, accuracy in bonding the IDEs to the fibres, and homogeneity of properties. The fibre is made of raw piezoelectric material (presently Morgan Matroc PZT-5H is being used at MIT's Active Materials and Structures Laboratory [21]). The circular fibre manufactured by CeraNova Corp. has a 0.13 mm diameter, and dimensions smaller than 0.10 mm are expected soon; the rectangular fibre, obtained by cutting monolithic ceramic sheets, can be manufactured down to 0.13×0.07 mm sections [18]. The piezoelectric properties of the specimen are determined by imposing one by one the boundary conditions pertaining to each independent strain and electric field conditions (i.e. the three unit extensions, the three unit shear deformation conditions, and the condition of unit electric field between two electrode sets) and computing the stress resultants. All these boundary conditions are required because the beam section analysis discussed later is based on the full three-dimensional properties of the material. The resulting properties of the equivalent material are reported in Table 1. Figures 2 and 3 respectively show the Von Mises stress and the detailed electric field due to a unit tension between the electrodes of the completely clamped specimen.

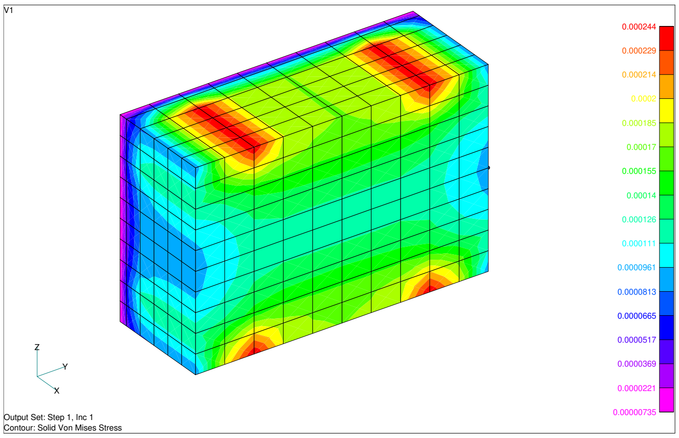

Figure 2: *Von Mises stress due to unit tension between the electrodes in rectangular fibre*

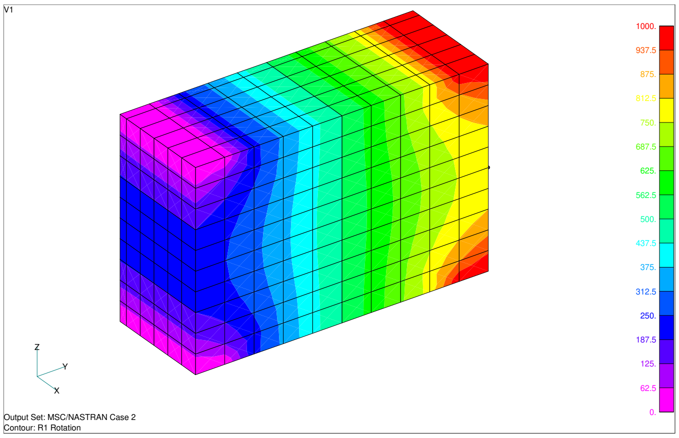

Figure 3: *Electric field due to unit tension between the electrodes in rectangular fibre*

Blade Section Characterisation

The beam model is very commonly used to model flexible rotor blades. It is easy to implement and to use, and at the same time it is able to describe the global behaviour of the blade with good accuracy. A beam model requires the knowledge of the elastic and piezoelectric properties of the passive and active parts of the active twist blade section; they are the constitutive matrices of linear piezoelectricity that express the internal forces and moments at each section of the beam as functions of the strains, the curvatures and the electric tensions on the electrodes. In the literature, these properties are usually estimated from the geometry of the structural part of the beam section, such as the area and the second order moments and the polar moment in the principal reference frame of the section [2]. This approach is valid for a very first approximation computation, and can lead to poor estimates of the stiffness properties when anisotropic materials are considered. Attempts to overcome this difficulty have been made by extending to the piezoelectric case a semi-monocoque (hollow) beam section analysis formulation, specialised to multi-cell configurations [3]. A rather sophisticated approach to the characterisation of the section of an anisotropic, non-homogeneous beam has been used in the present paper, based on an original formulation [14, 7] that has been extended to the analysis of beams embedding piezoelectric inclusions [8, 11]. It is based on a two-dimensional finite element discretisation of the section, that gives the user a great flexibility in the choice of the level of detail to be used in the characterisation. The displacements $s_{3\times1}$ at an arbitrary point $f_{3\times1} = [0, x, y]^T$ of the section are expressed as the combination of a warping displacement $g_{3\times1}$, superimposed to a reference rigid displacement and rotation of the whole section: $s = v(x) + g(x, y, z)$, being $v = Zr$ the reference displacements, where $Z_{3\times6} = [I_{3\times3}, -f\times]$ is a linearised rototranslation matrix, and $r_{6\times1}$ are the displacements and the rotations of the reference point of the section. The strains $S_{6\times1}$ at an arbitrary point depend on both the reference and the warping displacements; but while the reference displacements are functions of the position along the beam axis x only, the warping displacements depend also on the position in the beam section. The generalised deformations of the beam, $\psi_{6\times1}$, are expressed as functions of the derivatives of the reference displacements, i.e. $\psi = r_{/x} + \Pi r$, where the matrix $\Pi_{6\times6}$ adds the contribution of the section rotation to the shear strain, being:

$$\Pi = \begin{bmatrix} 0_{3\times3} & e_x\times \\ 0_{3\times3} & 0_{3\times3} \end{bmatrix}$$

where e_x is the unit vector in the direction of the beam axis, x. The warping displacement contribution to the strains is hidden in the section characterisation procedure. The warping displacements relax the overconstrained reference displacements, that are rigid in the plane of the section. This relaxation, in usual beam formulations, is accounted for by transforming the three-dimensional material properties into a uniaxial stress state; this naturally accounts for the unloaded side-surface boundary conditions in the axial and the bending load cases, while the torsion and the shear load cases usually require geometry depedent adjustments to account for the internal compatibility and for the boundary conditions, resulting in a roughly approximated, geometry-based description of the effects of the warping. In case of non-homogeneous beam sections, the equilibrium and compatibility conditions must be enforced also at the boundaries between different materials, while in the case of anisotropic materials, the strains due to a uniaxial stress state are fully coupled and imply a non-trivial warping solution. In this case the usual beam characterisation formulations fail even in the simpler cases of axial and bending loads. In the present formulation, the warping displacements are discretised in a finite element way by means of arbitrary shape functions that describe the displacements in terms of their nodal value; the nodal displacements retain the dependency on the axial abscissa: $g = N_{3\times3n}(y, z)\, u_{3n\times1}(x)$. The electric potential V, that represents the electric unknown, is described in analogy with the warping by means of the same shape functions: $V = N_{1\times n}(y, z)\, w_{n\times1}(x)$. The discretised strain and electric fields are:

$$\begin{cases} S = \partial_S\left(\psi, u, u_{/x}\right) \\ E = \partial_E\left(w, w_{/x}\right) \end{cases}$$

being $\partial_S(\cdot)$ and $\partial_E(\cdot)$ two linear differential operators. The virtual work principle, generalised to include the electric work made by charging the piezoelectrics, is used; the domain of integration is shown in Figure 4. The electric and the structural domains are not required to coincide, i.e. the host structure usually does not belong to the electric domain unless its dielectric properties are to be considered; the integration is intended to be performed only where the integrand fields are defined.

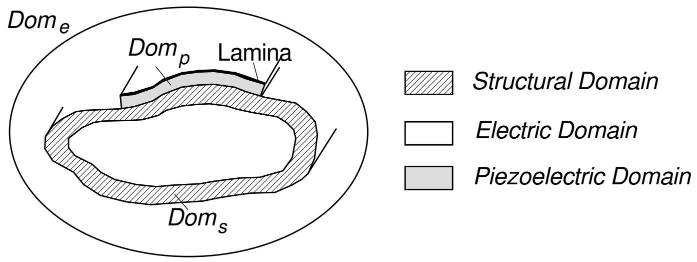

Figure 4: *Beam section*

The internal work per unit length is:

$$\delta L_{i/x} = \int_A \left(\delta S^T T + \delta E^T D \right) \, dA \tag{3}$$

where T and D are the stresses and electric displacements from Eq. 1. The external work is made of an electromechanical contribution that represents the transmission of the internal forces and of the dielectric displacement along the beam, i.e. the work made by the stresses and the dielectric displacement on the two surfaces obtained by cutting the slice of beam:

$$\delta L_{t/x} = \frac{\partial}{\partial x} \left(\int_A \left(\delta s^T p + \delta V^T q \right) \, dA \right) \tag{4}$$

being $p = T \cdot e_x$, $q = D \cdot e_x$ the stresses and the dielectric charge on the surface normal to the x axis. An external contribution comes from the work made by the polarisation charge on the electrodes of the piezoelectric devices:

$$\delta L_{e/x} = \int_c \delta V^T q_p \, dl \tag{5}$$

where q_p is the polarisation charge per unit length that is imposed on the electrodes c. The actual electric field in the AFC with IDEs varies along the fibre in an alternate manner, as shown in Fig. 3, as the polarisation direction does, but the averaged actuation behaviour is that of a uniformly polarised piezoelectric material subject to an in-plane constant electric field in direction 1 (material frame). The correct material behaviour is obtained by using the averaged material properties from the FEM analysis, while the effect of a constant electric field in direction 1 is obtained by applying a tension across the constant thickness of the piezoelectric plies (direction 3 in the material frame) and by switching the rows 1 and 3 of the piezoelectric matrix, $e = d \, {s^{(E)}}^{-1}$, of the AFC material. By carrying out the differentiations in Eq. 4, by equating the internal and external work expressions, Eq. 3 and Eqs. 4 and 5 respectively, and by operating some basic differentiations, the virtual work balance results in an expression of the form:

$$M_2 d_{/xx} + M_1 d_{/x} + M_0 d = F \tag{6}$$

where $d = \{u, w, \psi\}^T$ are the unknown nodal warpings and voltages and the generalised deformations of the sections. The expressions of the matrices M_0, M_1 and M_2 are not reported for the sake of conciseness[2]; they result from a standard finite element integration and assembly procedure. The right-hand term F contains the internal forces in the section under analysis, and the polarisation charge densities on the conductive laminæ, namely $F = [0, Q_c, \vartheta]^T$. By assuming constant polarisation charge densities and constant internal forces, with the exception of linear bending moments resulting from the constant transverse shears, i.e.:

$$F = \left\{ \begin{array}{c} 0 \\ Q_0 \\ \left(I_{6\times6} + x\Pi^T \right) \vartheta_0 \end{array} \right\} = \left(\left[\begin{array}{cc} 0 & 0 \\ I & 0 \\ 0 & I \end{array} \right] + x \left[\begin{array}{cc} 0 & 0 \\ \Pi^T & 0 \\ 0 & 0 \end{array} \right] \right) \left\{ \begin{array}{c} \vartheta_0 \\ Q_0 \end{array} \right\} = \left(H_0 + x H_1 \right) \Theta_0 \tag{7}$$

A solution of Eq. 6 in terms of linear influence coefficients related to unit internal forces at $x = 0$, ϑ_0, together with an analogous solution due to unit polarisation charges, Q_0, collected in the external loads unknown Θ_0 introduced in Eq. 7, can be determined for the warpings and the generalised deformations, i.e.:

$$\left\{ \begin{array}{lcl} d_s & = & \left(d_{0s} + x d_{1s} \right) \vartheta_0 \\ d_e & = & d_{0e} Q_0 \end{array} \right.$$

or:

$$d = \left(d_0 + x d_1 \right) \Theta_0 \tag{8}$$

Figure 5 shows the FEM model of the NACA 0012 airfoil that has been used in this analysis, while Figure 6 refers to the warping due to different mechanical and electric load conditions of the blade section under analysis.

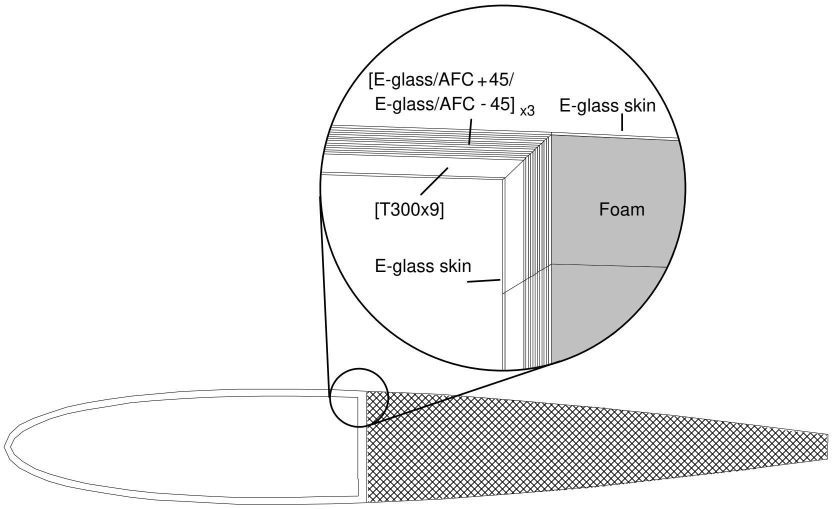

Figure 5: *Sketch of the blade section, with detail of the plies in the spar*

Mention should be made of the electric boundary conditions for the linear term of the structural solution: the electric potential on the conductors must be constant along the beam axis, thus a non-holonomic constraint on the axial derivatives of the tensions must be introduced, as highlighted in [11]. The elastic and piezoelectric properties are obtained by substituting the solution, Eq. 8, evaluated at $x = 0$, into the expression of the internal work, Eq. 3, written in the form of Eq. 6, resulting in:

$$\begin{aligned} \delta L_{i/x} &= \delta d^T \left(M_1 d_{/x} + M_0 d \right) \\ &= \delta \Theta_0{}^T d_0^T \left(M_1 d_1 + M_0 d_0 \right) \Theta_0 \\ &= \delta \Theta_0{}^T \mathcal{C} \Theta_0 \end{aligned}$$

where the generalised piezoelectric compliance matrix of the section, $\mathcal{C}$, is introduced; its inverse is the piezoelectric stiffness matrix $\mathcal{D} = \mathcal{C}^{-1}$. It can be decomposed in a 6×6 stiffness matrix K that in case of arbitrarily anisotropic, non-homogeneous materials will be fully coupled, a $N_e \times 6$ piezoelectric coupling matrix θ, N_e being the number of independent electrodes, and a $N_e \times N_e$ dielectric matrix. These matrices can be used in one's favourite finite element beam/truss analysis code; in this paper a finite volume formulation, implemented in a multibody, nonlinear dynamics code, has been used [13, 12].

Multibody Active Rotor Analysis

The detailed analysis of a helicopter rotor requires the ability to thoroughly describe the kinematics of finite, and possibly large, displacements and rotations. The traditional approach is based on dedicated comprehensive codes, that usually make some simplifying basic assumptions, such as considering the blade motion as the superimposition of local rigid rotations about the rotor hinges and of local flexible linear displacements, expressed in modal form, onto the rigid rotation, possibly at constant velocity, of the rotor. This approach is valid, efficient in terms of computational speed and cost, and it is surely able to describe the fundamental behaviour of the rotor; it can suffer from some limitations in case large rotations, nonlinear elastic behaviour or nonuniform rotation conditions are to be addressed. In this paper a rather different approach has been used, based on a multibody description of the whole rotor. No assumptions are made on the kinematics of the components of the rotor. The model is divided in independent bodies, that carry the lumped inertia of the system. The six equilibrium equations are written for each body in the global reference frame; the bodies are constrained by kinematic constraints and by flexible elements that

[2]The interested reader should consult Ref. [11]

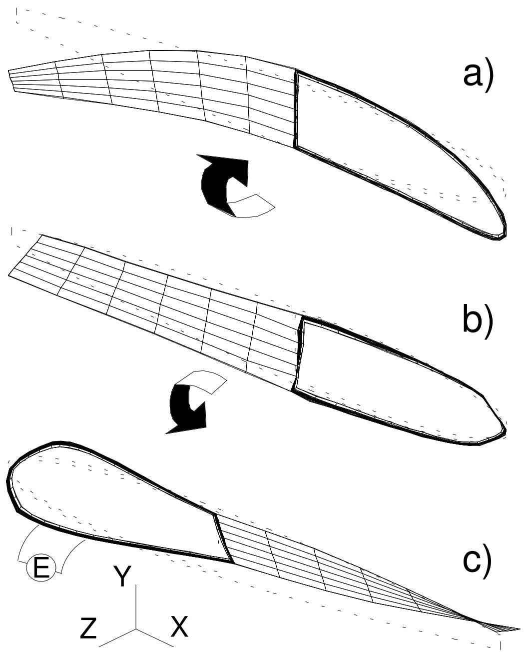

Figure 6: *Warpings due to (a) out-of-plane bending, (b) torsion, (c) electric tension that gives induced twist*

introduce configuration dependent forces. The kinematic constraints are accounted for by adding the algebraic constraint equations to the system, and by introducing the constraint reactions as unknowns in form of Lagrangian multipliers. Time integration is performed by an implicit linear multistep integrator that is unconditionally stable and allows the control of the algorithmic dissipation [12]. The rotor blades are modelled by finite volumes C^0 beams [13]; strip theory with dynamic stall, radial flow and Mach correction is used, in conjunction with dynamic inflow modelling [20]. As discussed in [10, 12], this approach allows a detailed analysis of the kinematics and of the dynamics of a rotorcraft avoiding any undue approximation in the kinematics of the system, and with the same order of refinement of a finite element model in the description of the flexibility, with reasonable and acceptable computational cost. The aerodynamic model is not as good as the structural one, though it is acceptable for most applications, and will be the object of further development.

Numerical Results

Model Description

The numerical analysis is based on an analytical model of the active twist rotor presented in Reference [22]. This is the analytical bench full-scale helicopter rotor the NASA Langley Research Center ATR wind tunnel model refers to [23, 24]. It is representative of a large class of medium weight helicopter rotors. The basic properties of the rotor are described in Table 2. Two analytical models have been studied in this paper, both based on the main properties of the mentioned rotor. The first one uses the same elastic and piezoelectric coefficients described in the mentioned paper, for direct comparison and model validation purposes. The second model is based on the proposed blade section characterisation method. The numerical results cannot be considered completely representative of the model they refer to, because the final active twist fitting of the ATR model is still under refinement. These results should be considered as a sample application of the proposed analysis procedure. Table 4 presents the structural properties resulting from this analysis com-

Table 2: *Rotor geometric and dynamic properties (Ref. [22])*

Symbol	Property	baseline	AFC blade
R	blade radius [in]	336	(same)
Ω	rotation speed [rad/s]	22.25	(same)
m	section mass, [lb-s^2/in/in]	1.11e-3	1.03e-3
c/R	nondimensional chord	0.0488	(same)
θ_1	linear pretwist [deg/R]	-8	(same)
γ	Lock number	9.77	(same)

Table 3: *Materials*

Property	glass-epoxy	graphite-epoxy	
c_{11}	2.15e6	26.36e6	[psi]
c_{12}	0.19e6	0.42e6	[psi]
c_{22}	1.98e6	1.50e6	[psi]
c_{66}	0.28e6	1.04e6	[psi]
ρ	6.50e-2	5.78e-2	[lbs/in^3]
thickness[a] h	5.10e-3	4.92e-3	[in]

[a]The thickness of the AFC plies is 5.50e-3 in.

pared to those given in Reference [22]; three different meshes of increasing refinement have been considered. The properties in Tab. 4 converge very quickly to their final value; the most challenging term is the position of the shear center, that travels from negative to positive as the mesh is refined. Further analyses with finer meshes confirmed that the presented value has converged to the final value. The AFC with rectangular fibre described in Tab. 1 has been used. The other materials used, namely $\pm45^o$ fiberglass (E-glass) for the outer skin and between the piezoelectric plies, and T300 unidirectional graphite-epoxy for the inner part of the spar, are described in Tab. 3. The laminate of the spar has been obtained by stacking, from the inner side, a ply of fiberglass, followed by 9 plies of T300 and by three sets of substacks made of fiberglass, $+45^o$ AFC, fiberglass and -45^o AFC. A final ply of fiberglass has been used to wrap the whole section, including the trailing part, that has been filled with foam, without any structural function; a schematic is shown in the detail of Figure 5. The thicknesses of the single plies are reported in Tab. 3. The spar goes from the leading edge to 40% of the blade chord; the piezoelectric plies are applied on the top and bottom surfaces approximately from 5% to 40% of the chord; in the web and in the nose the fiberglass is used instead of the AFC. The full stiffness and piezoelectric matrices obtained with the most refined mesh are reported in Table 5.

Table 4: *Stiffness properties (rectangular fibre)*

Stiffness		Mesh 1	Mesh 2	Mesh 3	Ref. [22]
Axial	[lb]	1.79e7	1.85e7	1.86e7	n.a.
Shear i.p.	[lb]	1.83e6	1.81e6	1.79e6	n.a.
Shear o.o.p.	[lb]	2.48e5	2.06e5	1.96e5	n.a.
Twist	[lb ft^2]	2.94e4	2.80e4	2.77e4	2.61e4
Bending o.o.p.	[lb ft^2]	6.89e4	7.07e4	7.11e4	9.16e4
Bending i.p.	[lb ft^2]	5.36e5	5.92e5	6.08e5	n.a.
Axial force center	[% chord]	2.28	2.79	2.96	0.00
Shear center	[% chord]	-1.68	1.26	2.18	0.00
Nodes		175	362	662	—
Elements		162	336	618	—

Table 5: *Stiffness and Piezoelectric matrices, ref. 25% chord; units: lb, ft and V.*

	Axial	Shear		Twist	Bending	
		i.p.	o.o.p.		i.p.	o.o.p.
Axial	1.86e+7	0.00e+0	1.91e+2	4.29e+2	0.00e+0	-7.53e+5
Shear i.p.		1.79e+6	0.00e+0	0.00e+0	-7.44e+1	0.00e+0
Shear o.o.p.			1.96e+5	5.85e+3	0.00e+0	-3.16e+2
Twist				2.77e+4	0.00e+0	-8.47e+1
Bending o.o.p.		sym.			7.11e+4	0.00e+0
Bending i.p.						6.08e+5
Piezo	0.00e+0	0.00e+0	1.29e-1	1.86e-1	0.00e+0	0.00e+0

Model Validation

A flexible model of the benchmark active twist rotor has been implemented. The model consists in the hub, a rigid body rotating at constant speed with respect to the ground, and carrying the hinges of the four blades. Coincident hinges for flap and lag have been considered, at 0.027 R from the rotation axis. A pitch bearing is placed right outwards of the hinges. The flexible blades are modelled by four three-node beam elements, with lumped inertia. The swashplate is modelled, with scissors to prevent the relative rotation about the rotor axis between the fixed plate and the ground, and between the rotating plate and the hub, with the three variable distance actuators from the ground to the fixed plate, and with fixed distance links from the rotating plate to each blade to impose the blade pitch. The model has been first validated from a dynamic standpoint by comparing the *in vacuo* rotating frequencies to those obtained in Ref. [22]. The frequencies have been obtained by system identification from the time domain response of the rotor subject to random excitation. The results are presented in Tab. 6. No lead-lag frequencies are presented, because no reference data is available for comparison. The first, rigid lead-lag frequency, due to an hinge offset of 9 in (0.027 R), is 0.20 Ω. The results from the model with beam properties taken from Ref. [22] are presented first, followed by those obtained with the beam properties estimated by the proposed procedure. The agreement on the lower flap frequencies is quite good because they are dominated by the centrifugal stiffness, while the fourth one obtained from the model with calculated stiffness properties is appreciably lower than in Ref. [22], due to the higher contribution of the structural stiffness to higher frequency flapping modes. The simplified, diagonal stiffness matrix

Table 6: *Comparison of in-vacuo rotating frequencies* [1/rev]

Mode	AFC blade			reference blade	
	MBDyn	MBDyn[a]	[22]	MBDyn	[22]
1st flap	1.02	1.02	1.02	1.02	1.02
2nd flap	2.59	2.58	2.62	2.61	2.62
3rd flap	4.69	4.55	4.79	4.67	4.79
4th flap	7.31	6.89	7.85	7.20	7.85
1st twist	3.31	3.38	3.38	6.48	6.16
2nd twist	9.65	10.0	9.78	18.4	18.3

[a]Stiffness properties from beam section analysis

commonly used, as in Ref. [22], represents a first approximation of the true stiffness properties of such a complicated beam, that can be useful for preliminary performance evaluation, but may cause underestimation of cross-coupling effects due for instance to the anisotropy of the materials. The importance of the cross-coupling coefficients, with particular regard to the dynamics of composite rotor blades, has been highlighted in [9]. The stiffness matrix reported in Tab. 5 shows significant couplings; some of them can be accounted for, in a conventional beam analysis, by applying offsets to the shear center or to the normal strain center, namely the couplings between twist and out-

Table 7: *Hover simulations with different stiffness properties*

		Ref. [22]	diagonal	coupled
Tip vertical displacement	[ft]	1.1053	1.1057	1.0343
Flap at flap hinge	[deg]	2.275	2.276	2.129
Elastic twist from root to tip	[deg]	-0.006	-0.005	-0.120
Thrust	[lb]	5.119e+03	5.133e+03	4.906e+03

of-plane shear, or the couplings between axial force and in-plane bending. Other couplings are strongly related to the anisotropy of the material, namely the coupling between axial and out-of-plane shear forces, and that between axial force and twist. A simple hover simulation, with 4° of collective pitch, has been performed first with the properties form Ref. [22], then with properties from the proposed analysis, both complete and "diagonalised" by neglecting the coupling terms. A comparison of some significant results is reported in Table 7.

Harmonic Actuation

The effectiveness of the active twist of the rotor blade has been investigated by performing analyses of the rotor in air with harmonic actuation of the blade. The hover condition is considered first. Root to tip twist, and root flap angles due to harmonic actuation of the active twist blade are reported in Figure 7 in the frequency range from 0.25 to 10 Ω. 250 V are applied to the electrodes of the AFC, corresponding to an average electric field of 33,000 V/in. The frequency response

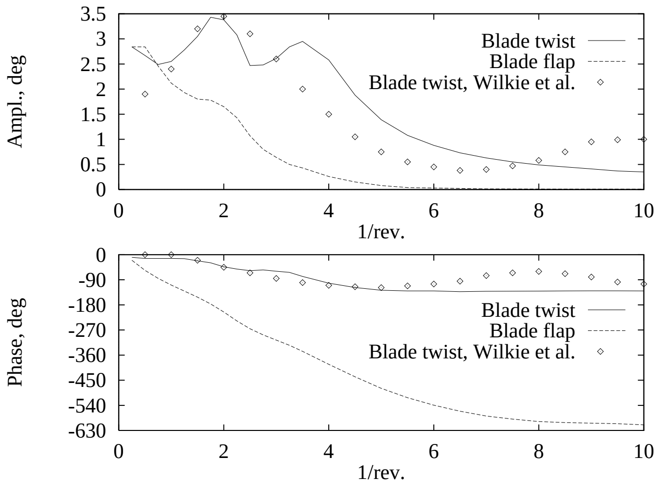

Figure 7: *Frequency response of root-to-tip twist and root flap at maximum control voltage*

shows a peak at about 3.5/rev. corresponding to the first twist mode of the blade, that is slightly damped by the aerodynamics. Another peak at about 2/rev. results from the excitation of the first flexible flap mode of the blade, that resonates at a lower frequency due to the high aerodynamic damping of the flap modes. The blade twist from Ref. [22] does show the peak at 2/rev., but the first twist mode is missing, possibly due to the unsteady aerodynamics model used in the mentioned reference, that adds considerable aerodynamic damping to the pitch movement; in the present work, the pitch movement is mainly dampened by structural damping. As expected, the frequency response of the thrust (not shown) shows a peak at zero frequency, due to the steady change in pitch, and the two above mentioned peaks at 2/rev. and 3.5/rev.; it is nearly zero at 1.02/rev., because at the first, rigid flap frequency, all the work made by the aerodynamic forces is spent in rigidly flapping the blades. A primary goal for the active control of rotorcraft by controlling the pitch of the blades is to obtain an induced twist of the order of 2° in the range of

0–5 Ω [15, 22]; Fig. 7 clearly shows that the goal is achievable.
Forward flight conditions at different advancing ratios have been subsequently considered; open-loop 2/rev. actuation has been performed with the objective of reducing the vibrations at the mast induced by the steady forward flight. These vibrations mainly are 4/rev. due to the periodic forces generated by the four blades of the rotor; they can be cancelled by using 2/rev. actuation since 2/rev. pitch change causes 2/rev. flapping of the rotor, which in turn results in Coriolis forces in the plane of the rotor at twice the frequency of the flapping motion. Open loop control results are reported in Figures 8, 9, 10 at different advancing ratios ranging from 0.20 to 0.30; convergence at higher advancing ratios is difficult.

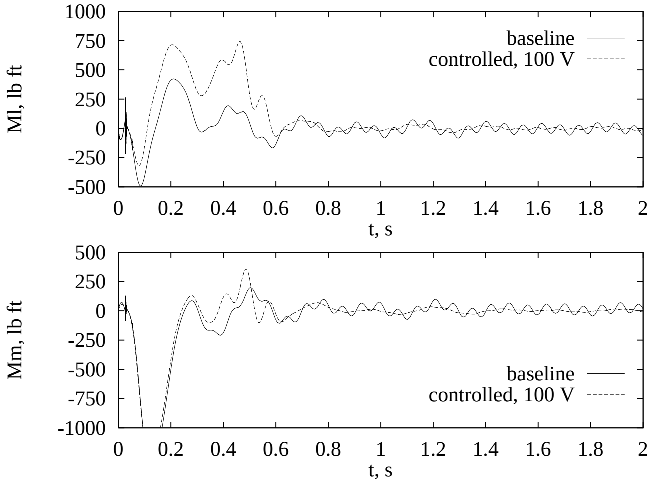

Figure 8: *Bending moments about x and y axes at the mast; advancing ratio $\mu = 0.20$; actuating tension: 100 V (40% of allowable) at 2/rev.; 131° phase shift*

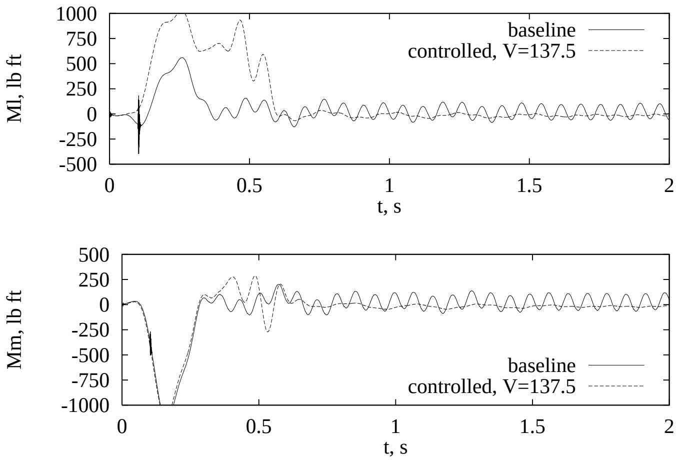

Figure 9: *Bending moments about x and y axes at the mast; advancing ratio $\mu = 0.25$; actuating tension: 137.5 V (55% of allowable) at 2/rev.; 128° phase shift*

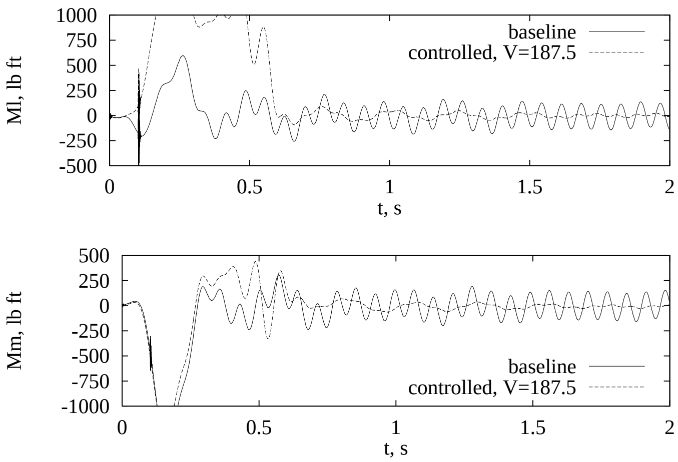

Figure 10: *Bending moments about x and y axes at the mast; advancing ratio $\mu = 0.30$; actuating tension: 187.5 V (75% of allowable) at 2/rev.; 127° phase shift*

Conclusions

A formulation for the characterisation of a blade section with embedded piezoelectric devices has been established; it has been used to determine the stiffness and piezoelectric properties of the blade of an Active Twist Rotor analytical model. A procedure based on Finite Element Analysis has been used to characterise the Active Fibre Composite piezoelectric material with Inter-Digitated Electrodes that is required to obtain in-plane anisotropic strain induction, and thus rotor blade twist induction. Multi-body analysis is being used to investigate the behaviour of the Active Twist Rotor in vibration suppression by open- and close-loop control in the frame of a global modelling approach. Partial results on the ability of the active twisting in reducing the airloads transmitted by the rotor have been illustrated. The predicted properties of the AFC blade show good agreement with available analytical data, and moreover they give a deeper insight into the properties of a composite piezoelectric beam in terms of stiffness cross-couplings. The proposed approach to the analysis of actively twisted rotor blades is able to analyse the complex operating conditions of an actively controlled rotorcraft to a comparatively high degree of refinement. The active twisting of the blade represents and interesting and very promising means for the active control of the dynamics of a rotor.

References

[1] Bent, A. A., N. W. Hagood, and J. P. Rodgers, 1995, “Anisotropic Actuation with Piezoelectric Fiber Composites”, *JoIMS&S*, Vol. 6, May

[2] Carpenter, M. J., 1997, “Using Energy Methods to Derive Beam Finite Elements Incorporating Piezoelectric Materials”, *J. Intell. Mat. Systems & Structures*, Vol. 1

[3] Cesnik, C., and S. Shin, 1998, “Structural Analysis for Designing Rotor Blades with Integral Actuators”, *Proceedings of 39th AIAA Structures, Structural Dynamics and Materials Conferences*, Long Beach

[4] Chen, T., 1994, “Micromechanical Estimates of the Overall Theroelectroelastic Moduli of Multiphase Fibrous Composites”, *Intl. J. Solids Structures*, Vol. 31, No. 22

[5] Dunn, M. L., and M. Taya, 1993, “Micromechanics Predictions of the Effective Electroelastic Moduli of Piezoelectric Composites”, *Intl. J. Solids Structures*, Vol. 30, No. 2

[6] Dunn, M. L., 1995, "A Theoretical Framework for the Analysis of Thermoelectroelastic Heterogeneous Media with Applications", *J. Intell. Mat. Systems & Structures*, Vol. 6, March

[7] Ghiringhelli, G. L., and P. Mantegazza, 1994, "Linear, Straight and Untwisted Anisotropic Beam Section Properties from Solid Finite Elements", *Composites Engineering*, Vol. 4, No. 12

[8] Ghiringhelli, G. L., P. Mantegazza, and P. Masarati, 1996, "Numerical Modelling of Anisotropic Non Homogeneous Beams with Embedded Piezoelectric Sensors and Actuators", 7^{th} *International Conference on Adaptive Structures and Technologies*, Sept. 23–25, Rome, Italy

[9] Ghiringhelli, G. L., and M. Lanz, 1997, "Dynamic Optimisation of Bearingless Helicopter Rotors", *CEAS International Forum on Aeroelasticity and Structural Dynamics*, June 17–20, Rome, Italy

[10] Ghiringhelli, G. L., P. Masarati, and P. Mantegazza, 1997, "Multi-Body Aeroelastic Analysis of Smart Rotor Blades, Actuated by Means of Piezo-Electric Devices", *CEAS International Forum on Aeroelasticity and Structural Dynamics*, June 17–20, Rome, Italy

[11] Ghiringhelli, G. L., P. Masarati, and P. Mantegazza, 1997, "Characterisation of Anisotropic, Non-Homogeneous Beam Sections with Embedded Piezo-Electric Materials", *J. Intell. Mat. Systems & Structures*, Vol. 8, No. 10, October, pp. 842–858

[12] Ghiringhelli, G. L., P. Masarati, P. Mantegazza, and M. W. Nixon, 1998, "Multi-Body Analysis of a Tiltrotor Configuration", Presented at the 7^{th} *Conference of Nonlinear Vibrations, Stability, and Dynamics of Structures*, July 26–30, Blacksburg, VA

[13] Ghiringhelli, G. L., P. Masarati, and P. Mantegazza, "A Multi-Body Implementation of Finite Volume C^0 Beams", accepted for publication on the *AIAA Journal*

[14] Giavotto, V., M. Borri, P. Mantegazza, G. L. Ghiringhelli, V. Caramaschi, G. C. Maffioli, F. Mussi, 1983, "Anisotropic Beam Theory and Applications", *Computers & Structures*, Vol. 16 No. 1-4

[15] Giurgiutiu, V., Z. Chaudry, and C. A. Rogers, 1995, "Engineering Feasibility of Induced Strain Actuators for Rotor Blade Active Vibration Control", *J. Intell. Mat. Systems & Structures*, Vol. 6, September

[16] Hagood, N., R. Kindel, K. Ghandi, and P. Gaudenzi, 1993, "Improving Transverse Actuation of Piezoceramics Using Interdigitated Surface Electrodes", *SPIE Smart Structures and Materials Conference*, Vol. 1917, Part 1, Feb. 1–4, pp. 341–352

[17] 1978, *IEEE Standards on Piezoelectricity*, IEEE std., 176

[18] Janos, B. Z., and N. W. Hagood, 1998, "Overview of Active Fiber Composites Technologies", Proceedings of the *6th International Conference on new Actuators - ACTUATOR98*, June '98, Bremen, Germany

[19] Masarati, P. and P. Mantegazza, 1997, "On the C^0 Discretisation of Beams by Finite Elements and Finite Volumes", *l'Aerotecnica Missili e Spazio*, Vol. 75, pp. 77–86

[20] Pitt, M., and Peters, D. A., 1981, "Theoretical Prediction of Dynamic-Inflow Derivatives", *Vertica*, Vol. 5

[21] Rodgers, J. P., and N. W. Hagood, 1998, "Preliminary Mach-Scale Hover Testing of an Integral Twist-Actuated Rotor Blade", *SPIE Conference*, San Diego, March 1–5

[22] Wilkie, W. K., K. C. Park, and W. K. Belvin, 1998, "Helicopter Dynamic Stall Suppression Using Piezoelectric Active Fiber Composite Rotor Blades", *AIAA-98-2002*

[23] Wilkie, W. K., P. H. Mirick, and C. W. Langston, 1997, "Rotating Shake Test and Modal Analysis of a Model Helicopter Rotor Blade", *NASA T.M. 4760*

[24] Wilkie, W. K., M. L. Wilbur, P. H. Mirick, C. E. Cesnik, S. Shin, 1999, "Aeroelastic Analysis of the NASA/Army/MIT Active Twist Rotor", Presented at the *55^{th} Annual Forum of the American Helicopter Society*, May 25–27, Montreal, Canada